

$LnCu_3(OH)_6Cl_3$ (Ln = Gd, Tb, Dy): Heavy lanthanides on spin-1/2 kagome magnets

Ying Fu(付盈), Lianglong Huang(黄良龙), Xuefeng Zhou(周雪峰), Jian Chen(陈见), Xinyuan Zhang(张馨元), Pengyun Chen(陈鹏允), Shanmin Wang(王善民), Cai Liu(刘才), Dapeng Yu(俞大鹏), Hai-Feng Li(李海峰), Le Wang(王乐), and Jia-Wei Mei(梅佳伟)

Citation: Chin. Phys. B, 2021, 30 (**10**): 100601. DOI: 10.1088/1674-1056/ac1e20
Journal homepage: http://cpb.iphy.ac.cn; http://iopscience.iop.org/cpb

What follows is a list of articles you may be interested in

Doping effect on the structure and physical properties of quasi-one-dimensional compounds $Ba_9Co_3(Se_{1-x}S_x)_{15}$ (x = 0-0.2)

Lei Duan(段磊), Xian-Cheng Wang(望贤成), Jun Zhang(张俊), Jian-Fa Zhao(赵建发), Wen-Min Li(李文敏), Li-Peng Cao(曹立朋), Zhi-Wei Zhao(赵志伟), Changjiang Xiao(肖长江), Ying Ren(任瑛), Shun Wang(王顺), Jinlong Zhu(朱金龙), and Chang-Qing Jin(靳常青)

Chin. Phys. B, 2021, 30 (**10**): 106101. DOI: 10.1088/1674-1056/ac1f03

Grain size and structure distortion characterization of α-MgAgSb thermoelectric material by powder diffraction

Xiyang Li(李西阳), Zhigang Zhang(张志刚), Lunhua He(何伦华), Maxim Avdeev, Yang Ren(任洋), Huaizhou Zhao(赵怀周), and Fangwei Wang(王芳卫)†

Chin. Phys. B, 2020, 29 (**10**): 106101. DOI: 10.1088/1674-1056/aba09c

Synthesis, structure, and properties of $Ba_9Co_3Se_{15}$ with one-dimensional spin chains

Lei Duan(段磊), Xian-Cheng Wang(望贤成), Jun Zhang(张俊), Jian-Fa Zhao(赵建发), Li-Peng Cao(曹立朋), Wen-Min Li(李文敏), Run-Ze Yu(于润泽), Zheng Deng(邓正), Chang-Qing Jin(靳常青)

Chin. Phys. B, 2020, 29 (**3**): 036102. DOI: 10.1088/1674-1056/ab69ea

Crystal structure and magnetic properties of disordered alloy $ErGa_{3-x}Mn_x$

Cong Wang(王聪), Yong-Quan Guo(郭永权), Shuo-Wang Yang(杨硕望)

Chin. Phys. B, 2019, 28 (**8**): 086101. DOI: 10.1088/1674-1056/28/8/086101

Isostructural phase transition-induced bulk modulus multiplication in dopant-stabilized ZrO_2 solid solution

Min Wang(王敏), Wen-Shu Shen(沈文舒), Xiao-Dong Li(李晓东), Yan-Chun Li(李延春), Guo-Zhao Zhang(张国召), Cai-Long Liu(刘才龙), Lin Zhao(赵琳), Shu-Peng Lv(吕舒鹏), Chun-Xiao Gao(高春晓), Yong-Hao Han(韩永昊)

Chin. Phys. B, 2019, 28 (**7**): 076109. DOI: 10.1088/1674-1056/28/7/076109

$LnCu_3(OH)_6Cl_3$ (Ln = Gd, Tb, Dy): Heavy lanthanides on spin-1/2 kagome magnets*

Ying Fu(付盈)[1,2], Lianglong Huang(黄良龙)[3], Xuefeng Zhou(周雪峰)[3], Jian Chen(陈见)[3], Xinyuan Zhang(张馨元)[4], Pengyun Chen(陈鹏允)[5], Shanmin Wang(王善民)[3], Cai Liu(刘才)[2], Dapeng Yu(俞大鹏)[2], Hai-Feng Li(李海峰)[1,†], Le Wang(王乐)[2,‡], and Jia-Wei Mei(梅佳伟)[2,6,§]

[1] *Joint Key Laboratory of the Ministry of Education, Institute of Applied Physics and Materials Engineering, University of Macau, Avenida da Universidade, Taipa, Macao SAR* 999078, *China*

[2] *Shenzhen Institute for Quantum Science and Engineering, and Department of Physics, Southern University of Science and Technology, Shenzhen* 518055, *China*

[3] *Department of Physics, Southern University of Science and Technology, Shenzhen* 518055, *China*

[4] *Institute of Functional Crystals, Tianjin University of Technology, Tianjin* 300384, *China*

[5] *Institute of Resources Utilization and Rare-earth Development, Guangdong Academy of Sciences, Guangzhou* 51065, *China*

[6] *Shenzhen Key Laboratory of Advanced Quantum Functional Materials and Devices, Southern University of Science and Technology, Shenzhen* 518055, *China*

(Received 19 July 2021; revised manuscript received 9 August 2021; accepted manuscript online 17 August 2021)

The spin-1/2 kagome antiferromagnets are key prototype materials for studying frustrated magnetism. Three isostructural kagome antiferromagnets $LnCu_3(OH)_6Cl_3$ (Ln = Gd, Tb, Dy) have been successfully synthesized by the hydrothermal method. $LnCu_3(OH)_6Cl_3$ adopts space group $P\bar{3}m1$ and features the layered Cu-kagome lattice with lanthanide Ln^{3+} cations sitting at the center of the hexagons. Although heavy lanthanides (Ln = Gd, Tb, Dy) in $LnCu_3(OH)_6Cl_3$ provide a large effective magnetic moment and ferromagnetic-like spin correlations compared to light-lanthanides (Nd, Sm, Eu) analogues, Cu-kagome holds an antiferromagnetically ordered state at around 17 K like $YCu_3(OH)_6Cl_3$.

Keywords: kagome lattice, hydrothermal method, frustrated magnetism, spin-1/2

PACS: 06.60.Ei, 61.05.cp, 75.10.Jm, 75.40.Cx **DOI:** 10.1088/1674-1056/ac1e20

1. Introduction

The kagome antiferromagnet (KAFM) has been intensively investigated both theoretically and experimentally as a long-standing platform to search for quantum spin liquid (QSL),[1–5] which is highly entangled quantum matter and features fractional excitations and no symmetry-breaking down to absolute zero temperature. Two famous KAFMs, herbertsmithite ($Cu_3Zn(OH)_6Cl_2$)[6,7] and Zn-barlowite ($Cu_3Zn(OH)_6FBr$),[8,9] have been regarded as the prototype for QSL. Both of them show no phase transition down to low temperatures and exhibit fractional spinon excitations revealed by inelastic neutron scattering (INS) and nuclear magnetic resonance (NMR). Beyond QSL, additional interactions like Dzyaloshinskii–Moriya (DM) interactions and single-ion anisotropies may lead KAFM into other exotic ground states. For example, V^{3+} ($S = 1$) ions in NaV_6O_{11}[10,11] build a kagome lattice and form spin-singlets. $KFe_3(OH)_6(SO_4)_2$ ($S = 5/2$)[12] presents a long-range order with positive chirality, while $CdCu_3(OH)_6(NO_3)_2$ ($S = 1/2$) forms 120° spin structure with negative chirality.[13,14] Theoretically, a suitable combination of geometric frustration, ferromagnetism, and spin–orbit interactions in kagome magnets would realize high-temperature fractional quantum hall states and superconducting state.[15–18] Experimentally, the Kondo physics scenario of non-magnetic impurities screened by spinons in QSL has been proposed according to the muon spin relaxation (μSR) study on $ZnCu_3(OH)_6SO_4$,[19] analogous to the Kondo effect usually observed in 3d–4f heavy fermion metals, where local spins are screened by itinerant electrons.

Recently, $YCu_3(OH)_6Cl_3$ with perfect Cu-kagome layers and free of the Y–Cu anti-site disorder has been proposed as an ideal quantum KAFM,[20] which has a "$\boldsymbol{q} = 0$" type (i.e., the magnetic unit cell is identical to the structural unit cell with uniform chirality) antiferromagnetic (AFM) order with negative chirality due to a large DM interaction.[21,22] Replacing yttrium with light lanthanides, $RCu_3(OH)_6Cl_3$ (R = Nd, Sm, Eu)

*Project supported by the Program for Guangdong Introducing Innovative and Entrepreneurial Teams (Grant No. 2017ZT07C062), Shenzhen Key Laboratory of Advanced Quantum Functional Materials and Devices (Grant No. ZDSYS20190902092905285), and Guangdong Basic and Applied Basic Research Foundation (Grant No. 2020B1515120100). L. Wang acknowledges the support of China Postdoctoral Science Foundation (Grant No. 2020M682780). H. F. Li acknowledges the financial supports from Science and Technology Development Fund, Macao SAR, China (File No. 0051/2019/AFJ), Guangdong Basic and Applied Basic Research Foundation (Guangdong-Dongguan Joint Fund No. 2020B1515120025), and Guangdong–Hong Kong–Macao Joint Laboratory for Neutron Scattering Science and Technology, China (Grant No. 2019B121205003).

†Corresponding author. E-mail: haifengli@um.edu.mo

‡Corresponding author. E-mail: wangl36@sustech.edu.cn

‡Corresponding author. E-mail: meijw@sustech.edu.cn

© 2021 Chinese Physical Society and IOP Publishing Ltd

compounds still show strongly frustrated behaviors in despite of forming the canted AFM order with Neel temperatures (T_N) ranging from 15 K to 20 K.[23,24] With expecting that the heavy rare earths may further affect the magnetic frustration, we synthesized the polycrystalline samples of $LnCu_3(OH)_6Cl_3$ (Ln = Gd, Tb, Dy) by a universal way. The magnetic susceptibilities and heat capacity were measured. We discussed the magnetic contributions of Cu-kagome lattice and heavy lanthanides. With these results, we conclude that the heavy lanthanides ions in $LnCu_3(OH)_6Cl_3$ have little impact on the intrinsic magnetism of kagome-Cu^{2+}.

2. Experimental details

Although the structure of $GdCu_3(OH)_6Cl_3$ was reported by Sun *et al.*[23] with tiny crystals, the high-purity sample was not obtained for further investigation of magnetic properties. In this work, we efficiently synthesized $LnCu_3(OH)_6Cl_3$ (Ln = Gd, Tb, Dy) samples with high purity by a hydrothermal method. The starting reagents were $GdCl_3{\cdot}6H_2O$ (99.9%, Alfa Aesar), $TbCl_3{\cdot}6H_2O$ (99.99%, Energy Chemical), $DyCl_3{\cdot}6H_2O$ (99.99%, Energy Chemical), and CuO (99.9%, Alfa Aesar). $LnCl_3{\cdot}6H_2O$ was ground thoroughly with CuO in a ratio of 1 : 3, and the mixture was transferred into an autoclave and heated at 200 ℃ for about 10 h. Finally, the blue polycrystallined powder of $LnCu_3(OH)_6Cl_3$ was obtained after washed repeatedly by alcohol. This method avoids impurities and is also suitable for the preparation of $YCu_3(OH)_6Cl_3$, $SmCu_3(OH)_6Cl_3$, and $EuCu_3(OH)_6Cl_3$.

The temperature-dependent powder x-ray diffraction (PXRD) was performed from $T = 300$ K to 4 K on Rigaku Smartlab-9 kW diffractometer with Cu K_α radiation ($\lambda_{K_{\alpha1}} = 1.54056$ Å, $\lambda_{K_{\alpha2}} = 1.54439$ Å, and intensity ratio $I_{K_{\alpha1}} : I_{K_{\alpha2}} = 2 : 1$). The scanning step width of 0.01° was applied to record the patterns in a 2θ range of 10°–100°. The structures of $LnCu_3(OH)_6Cl_3$ were refined by Rietveld profile methods using the FULLPROF suite of programs.[25] The magnetic and specific heat measurements of $LnCu_3(OH)_6Cl_3$ were performed with Quantum Design (QD) magnetic property measurement system (MPMS) SQUID magnetometer and physical property measurement system (PPMS), respectively.

3. Results and discussion

3.1. Crystal structure

The site disorder remains mired in controversy in this series of compounds. For $YCu_3(OH)_6Cl_3$, single-crystal diffraction revealed a splitting disorder of Y^{3+} and no anti-site disorder between Cu^{2+} and Y^{3+}.[20] However, the neutron scattering results[26] supported no splitting disorder for Y^{3+}. The no site-splitting for the rare earth ions was also proposed for $LnCu_3(OH)_6Cl_3$ (Ln = Nd, Sm, Gd, Eu).[23,24] In this experiment, we found no obvious improvement for the refinements after taking into account the splitting disorder for the rare earth ions. Therefore, we performed Rietveld profile refinement on $LnCu_3(OH)_6Cl_3$ (Ln = Gd, Tb and Dy) without considering the site-splitting of Ln^{3+}.

As shown in Figs. 1(a)–1(c), the good refinements for $LnCu_3(OH)_6Cl_3$ in space group $P\bar{3}m1$ (No. 164) suggest that

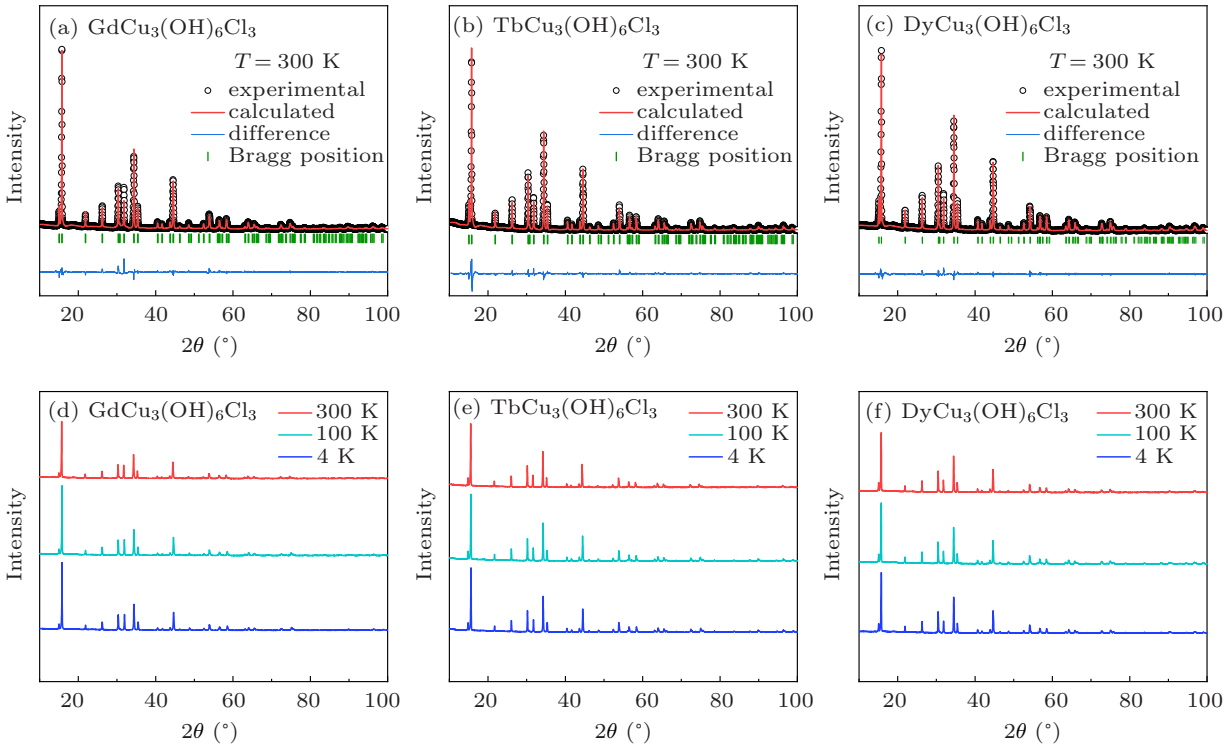


Fig. 1. Powder XRD patterns and refinements for $LnCu_3(OH)_6Cl_3$. (a)–(c) Refinements for PXRD at 300 K. (d)–(f) XRD patterns of $LnCu_3(OH)_6Cl_3$ at $T = 300$ K, 100 K, 4 K.

our powder sample is of high quality. The detailed lattice parameters are listed in Table 1. As excepted at 300 K, the lattice parameters decrease from Gd^{3+} to Dy^{3+} in coincidence with the decreasing of ion radius ($r = 1.053$ Å, 1.04 Å, 1.027 Å for Gd^{3+}, Tb^{3+}, Dy^{3+}, respectively). However, at 4 K, a and b show a contrast behavior with c, which is associated with the anisotropic thermal expansion. The temperature-dependent XRD patterns, as shown in Figs. 1(d)–1(f), have no peak-splitting or new peaks appearing as the temperature decreases down to 4 K, suggesting that no structure transition happens to $LnCu_3(OH)_6Cl_3$.

Table 1. Comparison of lattice parameters at 300 K and 4 K for $LnCu_3(OH)_6Cl_3$. $LnCu_3(OH)_6Cl_3$ is abbreviated to $LnCu_3$.

	300 K	4 K
$GdCu_3$	$a = b = 6.8019(47)$ Å	$a = b = 6.7923(65)$ Å
	$c = 5.6240(12)$ Å	$c = 5.5925(08)$ Å
	$R_{wp} = 9.47\%$	$R_{wp} = 10.0\%$
	$R_{Bragg} = 3.76\%$	$R_{Bragg} = 4.21\%$
$TbCu_3$	$a = b = 6.7888(35)$ Å	$a = b = 6.7797(91)$ Å
	$c = 5.6219(72)$ Å	$c = 5.5932(43)$ Å
	$R_{wp} = 13.1\%$	$R_{wp} = 13.7\%$
	$R_{Bragg} = 6.35\%$	$R_{Bragg} = 7.13\%$
$DyCu_3$	$a = b = 6.7655(98)$ Å	$a = b = 6.7631(14)$ Å
	$c = 5.6130(2)$ Å	$c = 5.6052(97)$ Å
	$R_{wp} = 6.61\%$	$R_{wp} = 6.61\%$
	$R_{Bragg} = 3.58\%$	$R_{Bragg} = 3.9\%$

As depicted in Fig. 2, each Cu^{2+} is surrounded by four equivalent O^{2-} and two Cl^-, forming a distorted $[CuO_4Cl_2]$ octahedron with the Cu–Cl bond (~ 2.82 Å) significantly longer than the Cu–O bond (~ 1.97 Å). The $[CuO_4Cl_2]$ octahedrons connect to each other by sharing the O–Cl edges to build the Cu-kagome plane. Ln^{3+} is 8-coordinated by six O^{2-} and two Cl^- to form $[LnO_6Cl_2]$ dodecahedron and locates at the center of the Cu-hexagon to constitute a Ln-triangular lattice (Fig. 2(c)).

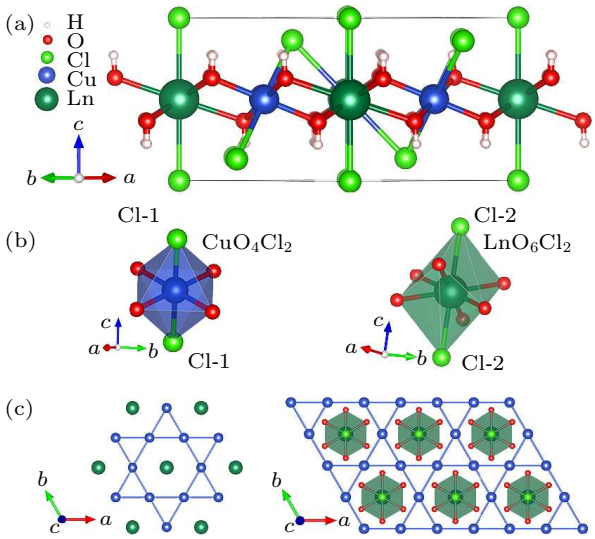


Fig. 2. Crystal structure of $LnCu_3(OH)_6Cl_3$ (Ln = Gd, Tb, Dy) without considering the site-splitting of Ln^{3+} ions. (a) Unit cell structure. (b) Coordinations of Cu and Ln atoms. (c) The illustration of Cu-kagome lattice and Ln-triangular lattice.

It is worth noting that analogous distorted octahedra $[CuO_4Cl_2]$ in herbertsmithite and $Y_3Cu_9(OH)_{19}Cl_8$ increase the splitting in the ligand-field of d orbitals and lower the energy level of d_{z^2} with a large d–d gap around 1–2 eV, unveiling the insulating nature of a charge transfer insulator,[27] which would be adapted to $YCu_3(OH)_6Cl_3$ and $LnCu_3(OH)_6Cl_3$.

The Cu–O–Cu super-exchange bond angles are $118.78(12)^\circ$ for $GdCu_3(OH)_6Cl_3$, $118.19(10)^\circ$ for $TbCu_3(OH)_6Cl_3$, and $117.7(4)^\circ$ for $DyCu_3(OH)_6Cl_3$, respectively. The values are comparable to the antiferromagnets like barlowite (117.4°)[28] and herbertsmithite (119°).[29] The Cu–Cu distances are 3.40330(11) Å for $GdCu_3(OH)_6Cl_3$, 3.39115(16) Å for $TbCu_3(OH)_6Cl_3$, and 3.3830(3) Å for $DyCu_3(OH)_6Cl_3$, equal to the corresponding Ln–Cu distance.

3.2. Magnetic properties

Figure 3 shows the temperature-dependent magnetizaion for $LnCu_3(OH)_6Cl_3$ (Ln = Gd, Tb, Dy), with $YCu_3(OH)_6Cl_3$ served as a reference. For $YCu_3(OH)_6Cl_3$ (Fig. 3(a)), the magnetic susceptibilities increase suddenly at 15 K, which is associated with the negative-vector-chirality 120° magnetic structure, confirmed by the neutron scattering study.[22] Continuously lowering the temperature, the drops at 3–4 K correspond to possible spin-glass state.[21] Compared to the small magnetic moment of Cu in $YCu_3(OH)_6Cl_3$, the magnetic susceptibilities of $LnCu_3(OH)_6Cl_3$ are much larger, suggesting that the dominant contribution to the magnetization arises from lanthanides, especially at low temperatures. As shown in Figs. 3(b)–3(d), under low fields, $LnCu_3(OH)_6Cl_3$ compounds present similar temperature-dependent magnetization curves as $YCu_3(OH)_6Cl_3$, with a rapid increase at about 16 K or 17 K and followed by a drop at lower temperatures. The zero field-cooling (ZFC) and field-cooling (FC) data at 0.005 T begin to split after the rapid increase, which could be ascribed to the possible in-plane canted ferromagnetic component, as previously pronounced in $RCu_3(OH)_6Cl_3$ (R = Nd, Sm, Eu).[23,24] It indicates that the Cu-kagome lattice of $LnCu_3(OH)_6Cl_3$ may have the same physics as $YCu_3(OH)_6Cl_3$, and form a magnetic structure at $T_N \sim 16$ K, which necessitates a neutron scattering study. In contrast to the robust magnetic order at 15 K in $YCu_3(OH)_6Cl_3$, the magnetic phase transition of $LnCu_3(OH)_6Cl_3$ can not be identified easily with increasing field. Whether T_N was suppressed by fields or the magnetic responses of Ln^{3+} ions masked the magnetic order of Cu^{2+} needs a further measurement of the specific heat.

As shown in Fig. 4, the high temperature behavior of the inverse magnetic susceptibility above 150 K was fit to the Curie–Weiss law $\chi = C/(T - \theta)$ (where C is the Curie constant, and θ is the Weiss temperature) in red lines with $C = 9.52$ K·emu·mol^{-1}, 13.76 K·emu·mol^{-1}, 16.05 K·emu·mol^{-1} and $\theta = -13.98$ K, -16.37 K, -13.72 K for Gd-, Tb-, and Dy-compounds, respectively. Considering the crystal-field

splitting for Ln^{3+} ions, we also applied the Curie–Weiss fitting between 20 K to 50 K, shown in black lines. The deduced θ are −1.71 K, −4.24 K, −1.40 K for $GdCu_3(OH)_6Cl_3$, $TbCu_3(OH)_6Cl_3$, and $DyCu_3(OH)_6Cl_3$, respectively. The absolute values of θ are smaller than those at high temperatures. The small Weiss temperatures are significant different from Nd-, Sm-, and Eu-analogues,[23,24] whose θ ranges from −100 K to −300 K with a distinct spin frustration compared to $T_N \sim 15$ K. Two main reasons for the reduction of θ are proposed: One is that the Cu–Cu AFM-interaction is weakened by Ln^{3+}; the other is that Ln^{3+} ions form a FM-interaction that competes with the Cu–Cu AFM-interaction.

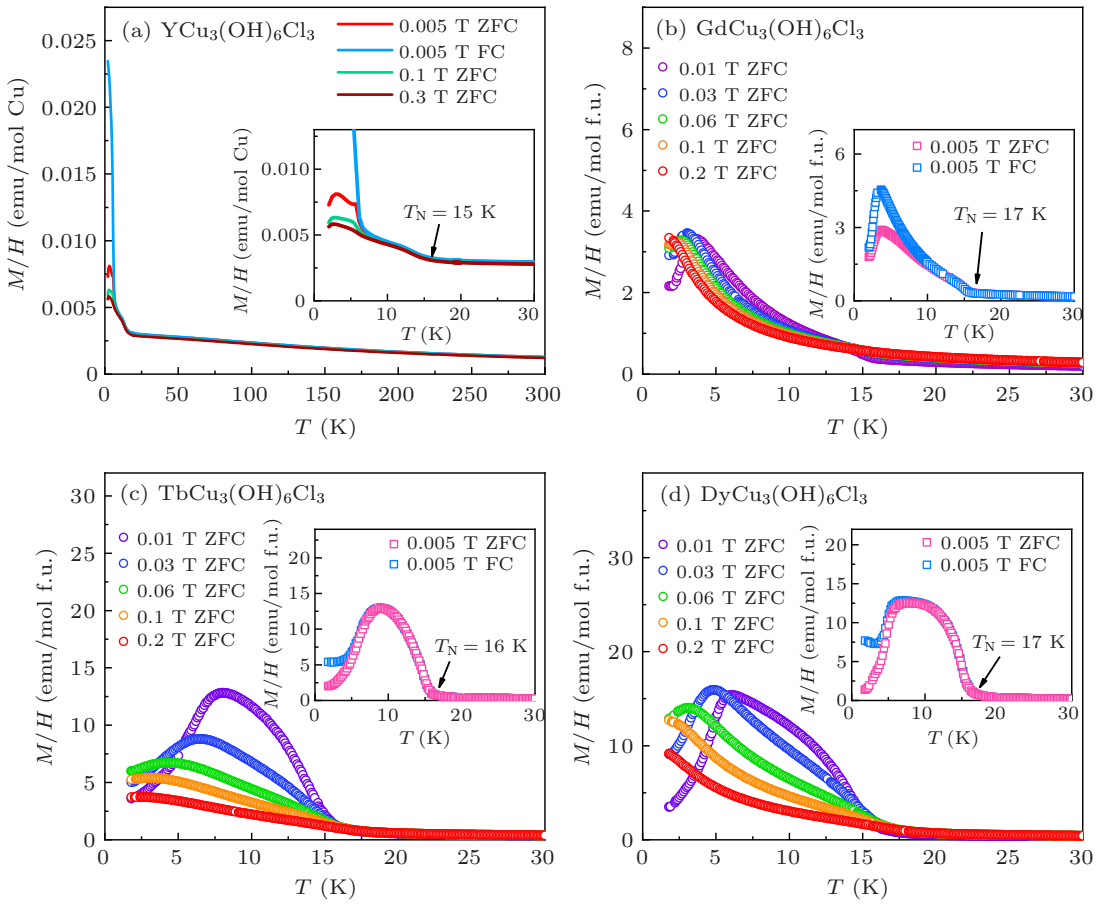


Fig. 3. Temperature-dependent magnetization of $YCu_3(OH)_6Cl_3$ and $LnCu_3(OH)_6Cl_3$ (Ln = Gd, Tb, Dy) at selected fields. Inset in (a) is the zoom-in data, and insets in (b)–(d) are the ZFC and FC curves collected at 0.005 T.

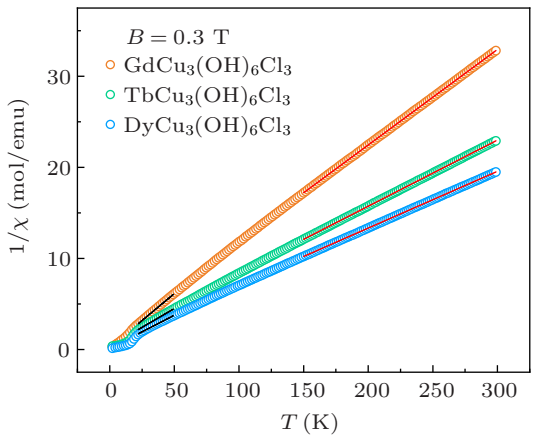


Fig. 4. Temperature dependence of inverse magnetic susceptibilities $1/\chi$ under a field of 0.3 T. The red and black lines are the fitting-plots of Curie–Weiss law at high temperatures (150–300 K) and low temperatures (20–50 K), respectively.

The effective magnetic moments μ_{eff} of $LnCu_3(OH)_6Cl_3$ deduced by the formula $\mu_{eff} = \sqrt{3k_BC/N_A}$ (where k_B is the Boltzmann constant, N_A is the Avogadro number, and C is the Curie constant) are 8.21 μ_B, 9.82 μ_B, and 10.45 μ_B for $GdCu_3(OH)_6Cl_3$, $TbCu_3(OH)_6Cl_3$, and $DyCu_3(OH)_6Cl_3$, respectively. For $LnCu_3(OH)_6Cl_3$, a system consisting two kinds of magnetic ions Ln^{3+} and Cu^{2+} (the theoretical effective magnetic moment for single ion is 1.73 μ_B for Cu^{2+}, 7.94 μ_B for Gd^{3+}, 9.72 μ_B for Tb^{3+}, and 10.63 μ_B for Dy^{3+}), the total theoretical effective magnetic moment can be roughly estimated by formula $\mu^t_{eff} = \sqrt{\mu^2_{Ln^{3+}} + 3\mu^2_{Cu^{2+}}}$, yielding $\mu^t_{GdCu_3} = 8.48\ \mu_B$, $\mu^t_{TbCu_3} = 10.17\ \mu_B$, and $\mu^t_{DyCu_3} = 11.04\ \mu_B$. Unlike $TbCu_3(OH)_6Cl_3$ and $DyCu_3(OH)_6Cl_3$, the effective magnetic moment of $GdCu_3(OH)_6Cl_3$ is close to the theoretical value, suggesting that Gd^{3+} is fully at the ground state due to the large crystal field-splitting energy $\Delta_{CEF} \gg 300$ K.

The field-dependent magnetization curves (M–H) of $LnCu_3(OH)_6Cl_3$ (Ln = Gd, Tb, Dy) are shown in Fig. 5, referred to $YCu_3(OH)_6Cl_3$ collected at 2 K. With decreasing temperature, the magnetization of $LnCu_3(OH)_6Cl_3$ in-

creases and grows rapidly below a field of about 2 T. At 2 K, $GdCu_3(OH)_6Cl_3$ saturates to a large value of 7.69 μ_B at 7 T, suggesting that spins of Gd^{3+} ions are polarized. $TbCu_3(OH)_6Cl_3$ and $DyCu_3(OH)_6Cl_3$ seem to be saturated with a linear increase under higher fields, especially for $DyCu_3(OH)_6Cl_3$, which could be ascribed to the temperature-independent Van Vleck paramagnetism. It is noted that the magnetic moment of each Cu^{2+} at 2 K is only 0.065 μ_B in the strong frustrated material, $YCu_3(OH)_6Cl_3$ ($\mu_0 H = 7$ T) (Fig. 5(a)), which is two orders of magnitude smaller than that of $LnCu_3(OH)_6Cl_3$. Thus, we deduce that lanthanide has a dominated magnetic contribution in $LnCu_3(OH)_6Cl_3$ at low temperatures and can easily dominate the magnetic response of the Cu-kagome lattice.

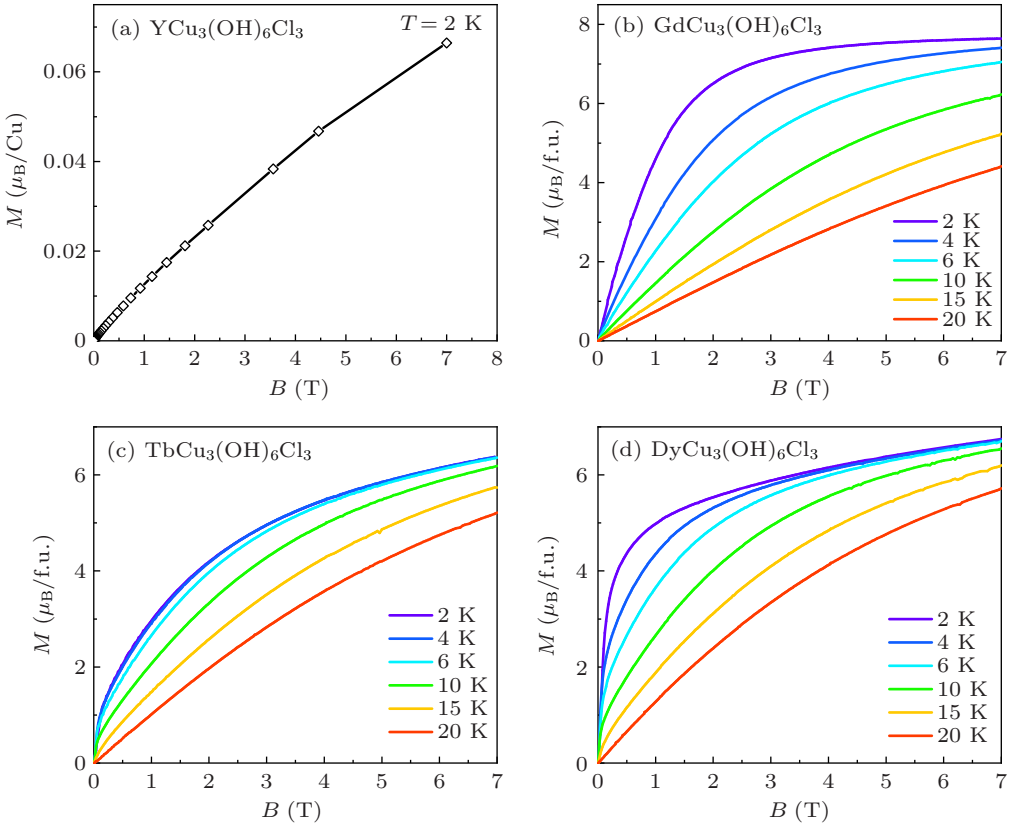


Fig. 5. Field-dependent magnetization of (a) $YCu_3(OH)_6Cl_3$ at 2 K and (b)–(d) $LnCu_3(OH)_6Cl_3$ (Ln = Gd, Tb, Dy) at selected temperatures.

3.3. Specific heat

Figure 6 shows the specific heat results of $LnCu_3(OH)_6Cl_3$ (Ln = Gd, Tb, Dy) and $YCu_3(OH)_6Cl_3$. As shown in Fig. 6(a), under zero field, a shoulder anomaly is observed at around 15–17 K for each compound, consistent with the rapid increase of magnetic susceptibilities at T_N, representing a formation of magnetic order for kagome-Cu^{2+}. Moreover, the low temperature (below 10 K) specific heat of $LnCu_3(OH)_6Cl_3$ shows more features, in contrast to decaying to zero for $YCu_3(OH)_6Cl_3$, relating to the low-temperature magnetic correlation of Ln^{3+} ions.

For further understanding the origin of the magnetic phase transition, we measured the specific heat with applied magnetic fields. Since the intrinsic nearest neighboring interaction in $YCu_3(OH)_6Cl_3$ is around 80 K,[30] the applied magnetic field (5 T) has little impact on the specific heat and entropy (see Figs. 6(b) and 6(c)), in line with previous report on $YCu_3(OH)_6Cl_3$[21] and $EuCu_3(OH)_6Cl_3$.[24] However, as shown in Figs. 6(d)–6(f), C_p/T of $LnCu_3(OH)_6Cl_3$ responses notably to the external magnetic field. For $GdCu_3(OH)_6Cl_3$, the upturn of C_p/T is generally evolved into a broad peak and pushed to high temperatures by field with T_N keeping constant. For $TbCu_3(OH)_6Cl_3$ and $DyCu_3(OH)_6Cl_3$, the low-temperature broad peak of C_p/T is efficiently pushed to above T_N by a field of 7 T and merges with the high-temperature broad peak induced by the magnetic phase transition. This behavior of driving the specific heat peak position to high temperatures by applied magnetic fields may indicate a formation of short-range ferromagnetic order below T_N.

Considering that $YCu_3(OH)_6Cl_3$ forms a robust $\boldsymbol{q} = 0$ type AFM order and $RCu_3(OH)_6Cl_3$ (R = Nd, Sm, Eu) enters a canted AFM phase below T_N, we speculated reasonably that $LnCu_3(OH)_6Cl_3$ (Ln = Gd, Tb, Dy) also has a canted AFM phase transition at T_N with a large ferromagnetic component. The ferromagnetic correlation is influenced obviously by fields and even screens the signal of AFM ordering in magnetic susceptibility, but the AFM phase indeed exists and is robust under large fields, like the case in $YCu_3(OH)_6Cl_3$.

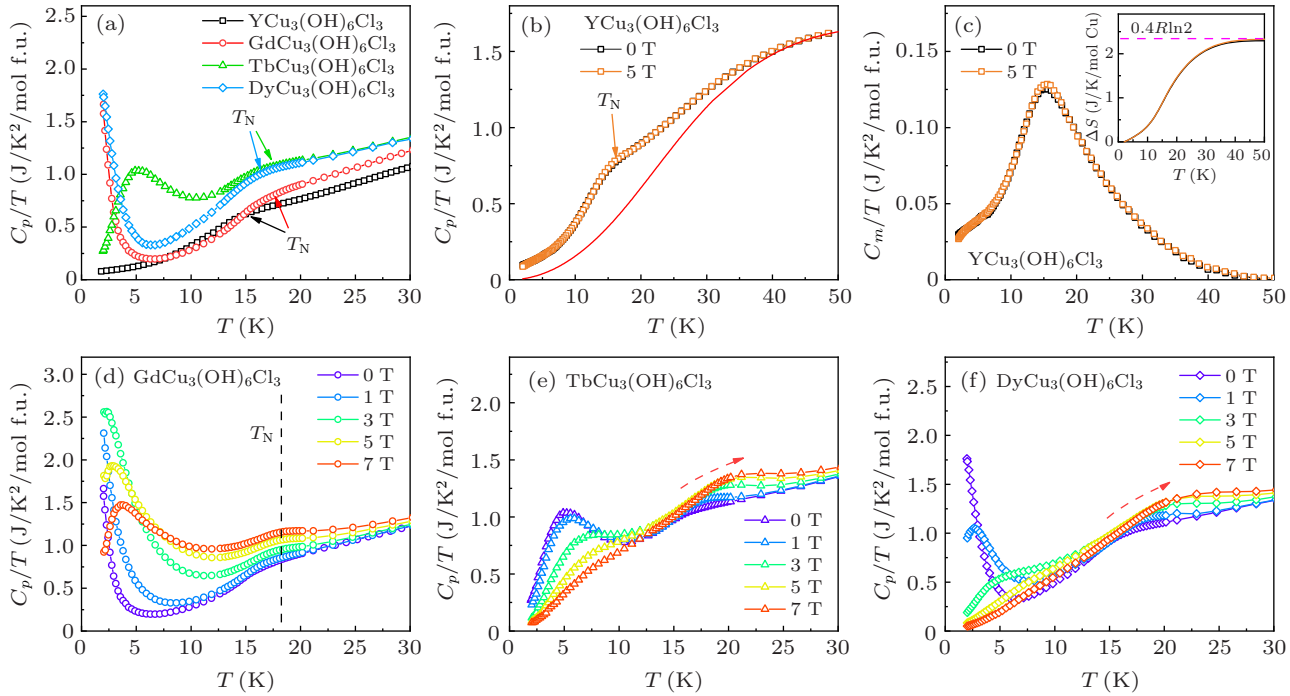


Fig. 6. Specific heat for $YCu_3(OH)_6Cl_3$ and $LnCu_3(OH)_6Cl_3$ (Ln = Gd, Tb, Dy). (a) C_p/T for $YCu_3(OH)_6Cl_3$ and $LnCu_3(OH)_6Cl_3$ under zero field. (b) The C_p/T of $YCu_3(OH)_6Cl_3$. The red solid line is phonon-contribution fitting. (c) Magnetic specific heat C_m/T of $YCu_3(OH)_6Cl_3$ after subtracting phonon-contribution. Inset is magnetic entropy per Cu^{2+}. (d)–(f) Temperature-dependent specific heat under different magnetic fields for $GdCu_3(OH)_6Cl_3$, $TbCu_3(OH)_6Cl_3$, and $DyCu_3(OH)_6Cl_3$, respectively.

3.4. Discussion and conclusion

The $\boldsymbol{q} = 0$ type magnetic structure with negative-chirality in $YCu_3(OH)_6Cl_3$ is interesting, which was also reported in other kapellasite-type compounds like $CdCu_3(OH)_6(NO_3)_2$ with T_N = 4 K[14] and $CaCu_3(OH)_6Cl_2$ with $T_N = 7.2$ K.[31,32] As demonstrated recently, with light lanthanides (Sm and Eu) replacing yttrium, $SmCu_3(OH)_6Cl_3$ and $EuCu_3(OH)_6Cl_3$ still feature canted antiferromagnetic ordering with strong spin frustration.[23,24] The light lanthanides with small magnetic moment may have limited influence on the magnetism of Cu-kagome lattice.

In our work, the magnetic and thermodynamic behaviors of $LnCu_3(OH)_6Cl_3$ (Ln = Gd, Tb, Dy) exhibit two significantly different characteristics: large magnetic moment compared with $YCu_3(OH)_6Cl_3$ and a ferromagnetic-like spin correlation below T_N. According to our experimental results, heavy lanthanides (Gd, Tb, Dy) probably modulate the DM interaction and induce a large ferromagnetic correlation, which can mask the intrinsic low-temperature magnetic properties of kagome-Cu^{2+}, but can not prevent the AFM ordering of Cu-kagome as revealed in specific heat. The Curie–Weiss law no longer works for evaluating the intrinsic interactions. The spectroscopy technology, like electron spin resonance (ESR) or μSR , is hopeful to further detect the detailed magnetic interactions for $LnCu_3(OH)_6Cl_3$ (Ln = Nd, Sm, Eu, Gd, Tb, Dy).

In summary, we have successfully synthesized the polycrystalline samples of $LnCu_3(OH)_6Cl_3$ (Ln = Gd, Tb and Dy). The heavy lanthanides significantly change the magnetic and thermodynamic behaviors, which keep the intrinsic magnetism of Cu-kagome lattice. $LnCu_3(OH)_6Cl_3$ (Ln = Nd, Sm, Eu, Gd, Tb, Dy) compounds provide a good platform to further investigate systemically the effect of lanthanides on the frustrated magnetism of Cu-kagome lattice.

Acknowledgement

We thank Dr. L. Zhang, Dr. J. M. Sheng, and Prof. L. S. Wu for useful discussion.

References

[1] Savary L and Balents L 2016 *Rep. Prog. Phys.* **80** 016502
[2] Broholm C, Cava R, Kivelson S, Nocera D, Norman M and Senthil T 2020 *Science* **367** 6475
[3] Feng Z, Yi W, Zhu K, Wei Y, Miao S, Ma J, Luo J, Li S, Meng Z Y and Shi Y 2018 *Chin. Phys. Lett.* **36** 017502
[4] Wen J J and Lee Y S 2019 *Chin. Phys. Lett.* **36** 50101
[5] Wei Y, Ma X, Feng Z, Adroja D, Hillier A, Biswas P, Senyshyn A, Hoser A, Mei J W, Meng Z Y, Luo H Q, Shi Y G and Li S L 2020 *Chin. Phys. Lett.* **37** 107503
[6] Helton J, Matan K, Shores M, Nytko E, Bartlett B, Yoshida Y, Takano Y, Suslov A, Qiu Y, Chung J H, Nocera D G and Lee Y S 2007 *Phys. Rev. Lett.* **98** 107204
[7] Han T H, Helton J S, Chu S, Nocera D G, Rodriguez-Rivera J A, Broholm C and Lee Y S 2012 *Nature* **492** 406
[8] Feng Z, Li Z, Meng X, Yi W, Wei Y, Zhang J, Wang Y C, Jiang W, Liu Z, Li S, Liu F, Luo J, Li S, Zheng G, Meng Z Y, Mei J W and Shi Y 2017 *Chin. Phys. Lett.* **34** 077502
[9] Feng Z, Wei Y, Liu R, Yan D, Wang Y C, Luo J, Senyshyn A, dela Cruz C, Yi W, Mei J W, Meng Z Y, Shi Y G and Li S 2018 *Phys. Rev. B* **98** 155127
[10] Seo D K and Whangbo M H 1996 *J. Am. Chem. Soc.* **118** 3951

[11] Kato H, Kato M, Yoshimura K and Kosuge K 2001 *J. Phys.: Condens. Matter* **13** 9311
[12] Inami T, Nishiyama M, Maegawa S and Oka Y 2000 *Phys. Rev. B* **61** 12181
[13] Nytko E A, Shores M P, Helton J S and Nocera D G 2009 *Inorg. Chem.* **48** 7782
[14] Okuma R, Yajima T, Nishio-Hamane D, Okubo T and Hiroi Z 2017 *Phys. Rev. B* **95** 094427
[15] Ribeiro P and Lee P A 2011 *Phys. Rev. B* **83** 235119
[16] Guterding D, Jeschke H O and Valentí R 2016 *Sci. Rep.* **6** 1
[17] Tang E, Mei J W and Wen X G 2011 *Phys. Rev. Lett.* **106** 236802
[18] Guo H M and Franz M 2009 *Phys. Rev. B* **80** 113102
[19] Gomilšek M, Žitko R, Klanjšek M, Pregelj M, Baines C, Li Y, Zhang Q and Zorko A 2019 *Nat. Phys.* **15** 754
[20] Sun W, Huang Y X, Nokhrin S, Pan Y and Mi J X 2016 *J. Mater. Chem. C* **4** 8772
[21] Zorko A, Pregelj M, Klanjšek M, Gomilšek M, Jagličić Z, Lord J, Verezhak J, Shang T, Sun W and Mi J X 2019 *Phys. Rev. B* **99** 214441
[22] Zorko A, Pregelj M, Gomilšek M, Klanjšek M, Zaharko O, Sun W and Mi J X 2019 *Phys. Rev. B* **100** 144420
[23] Sun W, Huang Y X, Pan Y and Mi J X 2017 *Dalton Trans.* **46** 9535
[24] Puphal P, Zoch K M, Dśor J, Bolte M and Krellner C 2018 *Phys. Rev. Mater.* **2** 063402
[25] Rodríguez-Carvajal J 1993 *Physica B* **192** 55
[26] Barthélemy Q, Puphal P, Zoch K M, Krellner C, Luetkens H, Baines C, Sheptyakov D, Kermarrec E, Mendels P and Bert F 2019 *Phys. Rev. Mater.* **3** 074401
[27] Pustogow A, Li Y, Voloshenko I, Puphal P, Krellner C, Mazin I I, Dressel M and Valentí R 2017 *Phys. Rev. B* **96** 241114
[28] Han T H, Singleton J and Schlueter J A 2014 *Phys. Rev. Lett.* **113** 227203
[29] Freedman D E, Han T H, Prodi A, Müller P, Huang Q Z, Chen Y S, Webb S M, Lee Y S, McQueen T M and Nocera D G 2010 *J. Am. Chem. Soc.* **132** 16185
[30] Arh T, Gomilšek M, Prelovšek P, Pregelj M, Klanjšek M, Ozarowski A, Clark S, Lancaster T, Sun W, Mi J X and Zorko A 2020 *Phys. Rev. Lett.* **125** 027203
[31] Yoshida H, Noguchi N, Matsushita Y, Ishii Y, Ihara Y, Oda M, Okabe H, Yamashita S, Nakazawa Y, Takata A, Kida T, Narumi Y and Hagiwara M 2017 *J. Phys. Soc. Jpn.* **86** 033704
[32] Iida K, Yoshida H K, Nakao A, Jeschke H O, Iqbal Y, Nakajima K, Ohira-Kawamura S, Munakata K, Inamura Y, Murai N, Ishikado M, Kumai R, Okada T, Oda M, Kakurai K and Matsuda M 2020 *Phys. Rev. B* **101** 220408